Investigating Gas Sorption in an rht-Metal–Organic Framework with 1,2,3-Triazole Groups

Katherine A. Forrest,[†,§] Tony Pham,[†,§] and Brian Space[*,†]
[†]*Department of Chemistry, University of South Florida,*
4202 East Fowler Avenue, CHE205, Tampa, FL 33620-5250, United States
[§]Authors contributed equally
[*]tpham4@mail.usf.edu; brian.b.space@gmail.com

Crystal Structure Comparison

Table S1. Comparison of the lattice parameters for the single X-ray crystal structures of Cu-BTTI as reported by three different groups.

Given Name	NTU-105	NOTT-122	NU-125
a (Å)	30.7992	30.926	31.3109
b (Å)	30.7992	30.926	31.3109
c (Å)	44.8105	45.103	44.807
α (°)	90	90	90
β (°)	90	90	90
γ (°)	90	90	90
Reference	1	2	3

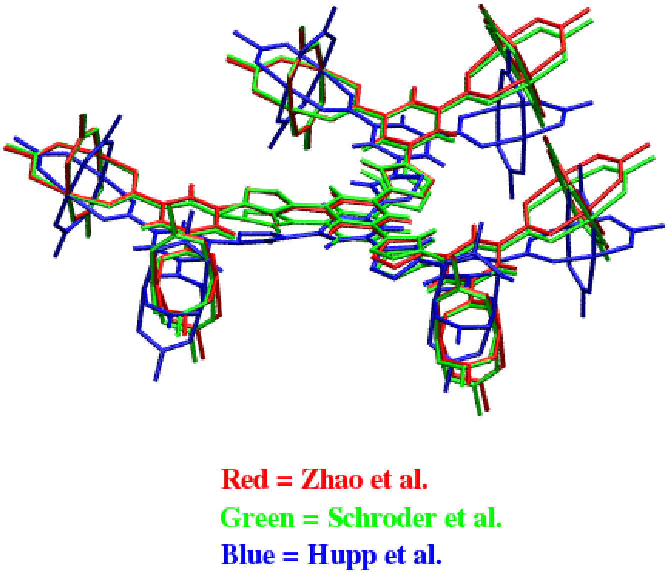

Figure S1. Comparison of the relative positions of the framework atoms for three different X-ray crystal structures of Cu-BTTI (Zhao *et al.* = red, Schröder *et al.* = green, Hupp *et al.* = blue). Note, the crystal structure reported by Schröder *et al.* contains disorder within the 1,2,3-triazole groups and central aromatic ring.

Parametrization

All atoms of Cu-BTTI were assigned Lennard-Jones 12–6 parameters (ϵ and σ),[4] point partial charges, and point polarizabilities to model repulsion/dispersion, stationary electrostatic, and many-body polarization interactions, respectively. In this work, the Lennard-Jones parameters for all C, H, N, and O atoms were taken from the Optimized Potentials for Liquid Simulations – All Atom (OPLS-AA) force field.[5] For Cu, the parameters from the Universal Force Field (UFF)[6] were used as the OPLS-AA force field does not contain such parameters for this atom. The interactions between unlike species were calculated using the Lorentz–Bertholet mixing rules.[7]

The partial charges for all chemically distinct atoms in Cu-BTTI were determined through electronic structure calculations on different representational fragments that were selected from the crystal structure of the MOF. More details of obtaining the partial charges for the unique atoms in Cu-BTTI are provided in the next section. The stationary electrostatic energy was calculated through Ewald summation[8,9] of the point partial charges. The exponential damping-type polarizabilities for all C, H, N, and O atoms were taken from reference 10, which contains a carefully parametrized and transferable set of polarizabilities for various light atoms and halogens. The polarizability for Cu^{2+} was determined in reference 11 and used herein. Classical polarization was included explicitly in the simulations using a Thole-Applequist type model.[12–15]

Electronic Structure Calculations

All electronic structure calculations were performed on the crystal structure of Cu-BTTI as reported in reference 1. Since there are four Cu^{2+} ions in chemically distinguishable environments and all atoms of the BTTI linker are unique, there are a total of 76 chemically distinct atoms in the crystal structure of the MOF (Figure S2). This served as the basis for selecting viable fragments for charge-fitting calculations for Cu-BTTI. The fragments that were selected for the charge-fitting calculations in this work are provided in Figure S3.

All calculations on each fragment of Cu-BTTI were performed at the Hartree–Fock level of theory using the NWChem *ab initio* simulation software.[16] For these calculations, all C, H, N, and O atoms were treated with the 6-31G* basis set, which has been shown to produce overpolarized charges that are appropriate for condensed phase simulation.[17] For the Cu^{2+} ions, the LANL2DZ effective core potential basis set[18–20] was used for proper treatment of the inner electrons of this metal species. The NWChem software was used to calculate the electrostatic potential surface (ESP) of each fragment. Afterward, the partial charges were fitted onto the atomic centers of the individual fragments through the CHELPG method[21] to reproduce the calculated ESP.

The partial charges for each chemically distinct atom were averaged between the selected fragments. We note that atoms that are buried or located on the edges of the fragments were not included in the averaging. Next, the partial charges were adjusted such that the total charge of the system was equal to zero. The resulting partial charges for each chemically distinct atom in Cu-BTTI after the adjustment can be found in Table S2. These partial charges were used for the simulations in this work to calculate permanent electrostatic interactions.

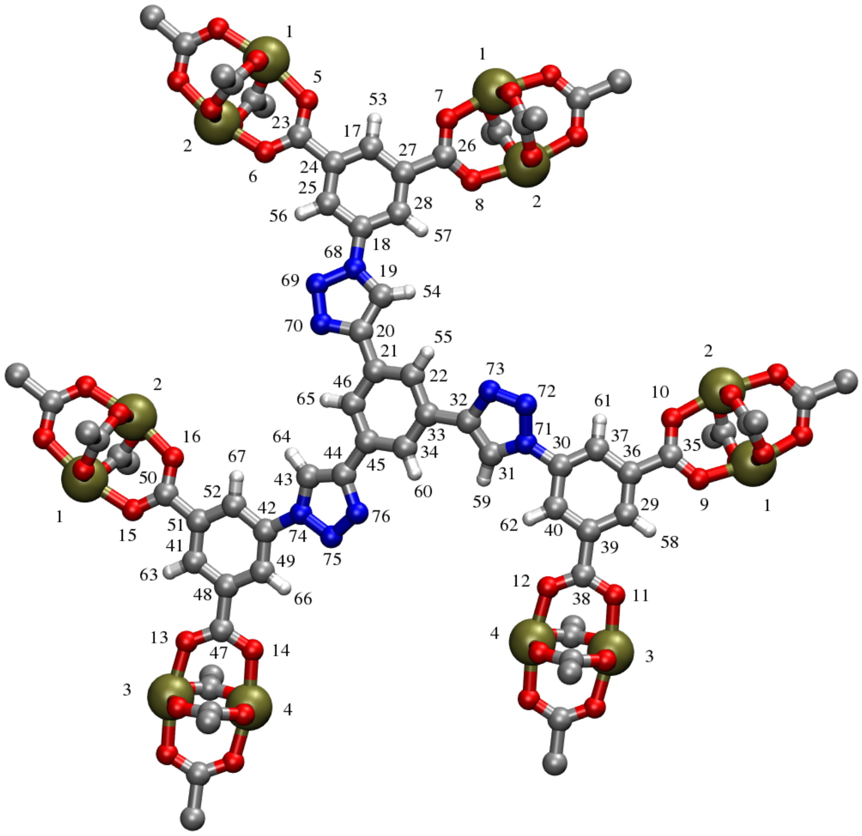

Figure S2. The numbering of the chemically distinct atoms in Cu-BTTI as referred to in Table S2. All atoms of the BTTI linker are chemically unique. The crystallographic distances between atom pairs 19–54, 31–59, and 43–64 are 0.94853, 0.94968, and 0.94889 Å, respectively. Atom colors: C = gray, H = white, O = red, Cu = tan.

Figure S3. Fragments of Cu-BTTI that were selected for gas phase charge fitting calculations. Atom colors: C = gray, H = white, N = blue, O = red, Cu = tan.

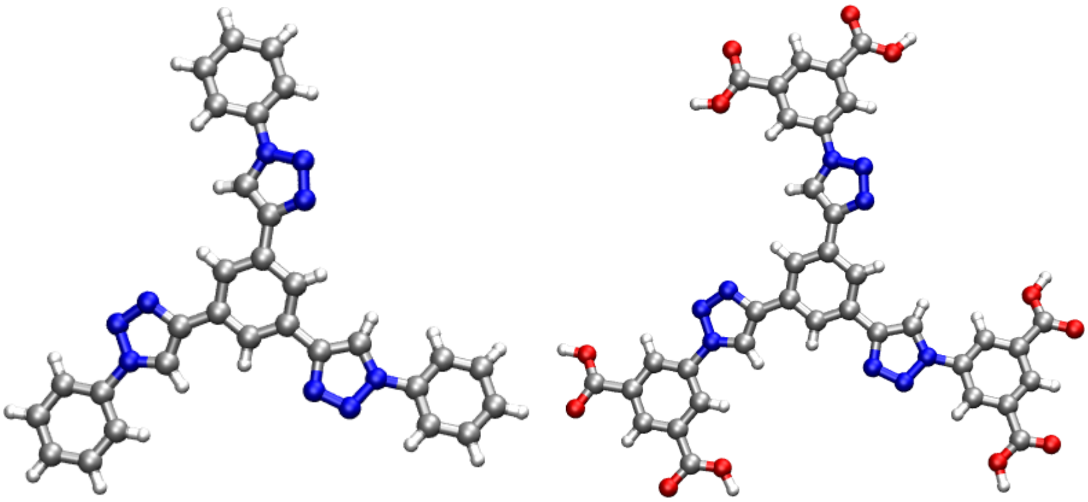

(a) Fragment 1 (b) Fragment 2

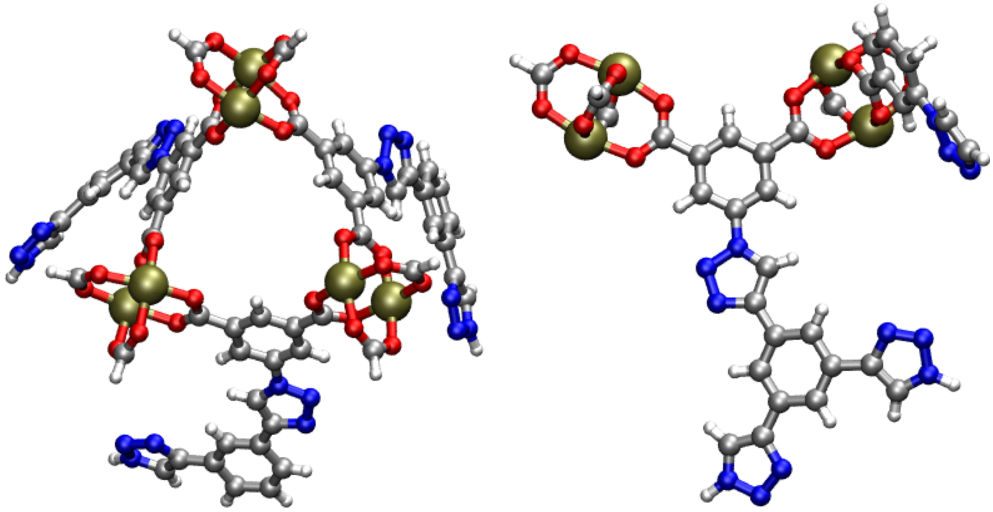

(c) Fragment 3 (d) Fragment 4

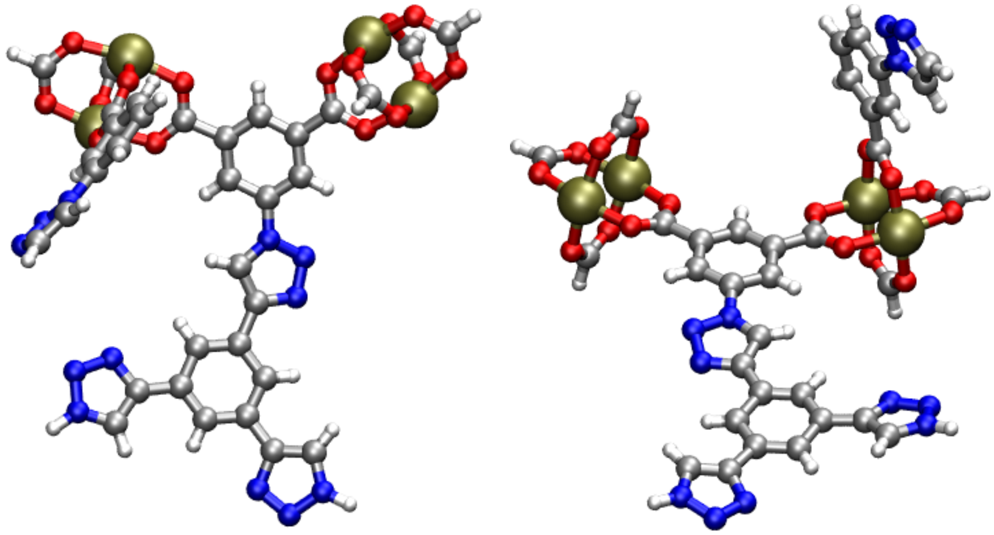

(e) Fragment 5 (f) Fragment 6

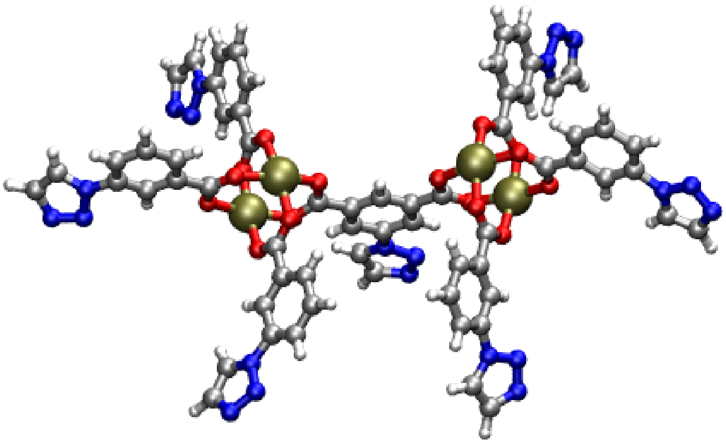

(g) Fragment 7

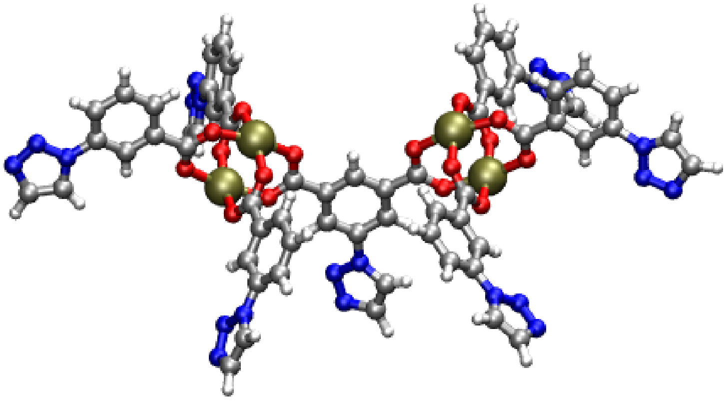

(h) Fragment 8

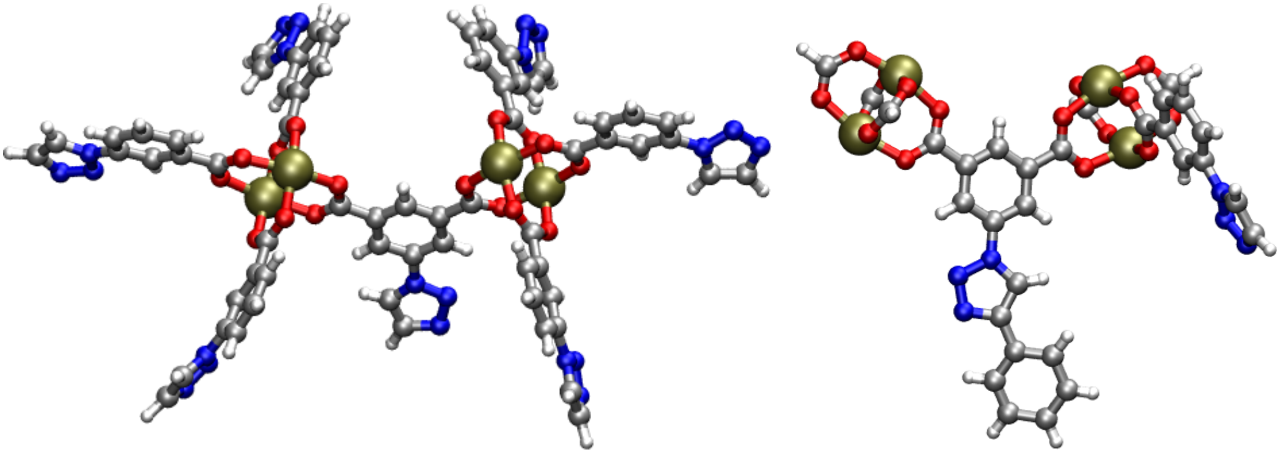

(i) Fragment 9

(j) Fragment 10

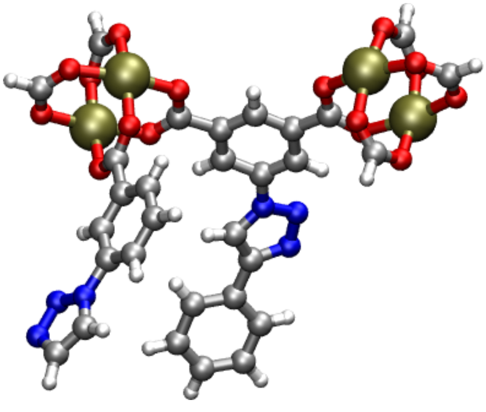

(k) Fragment 11

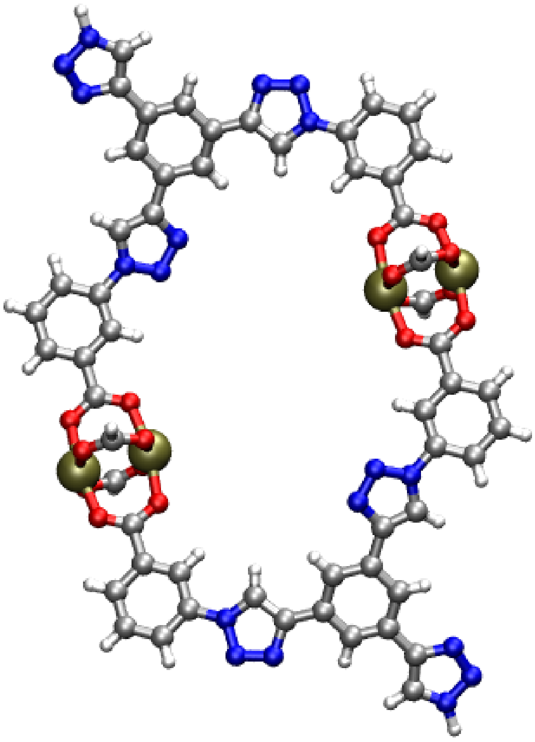

(l) Fragment 12

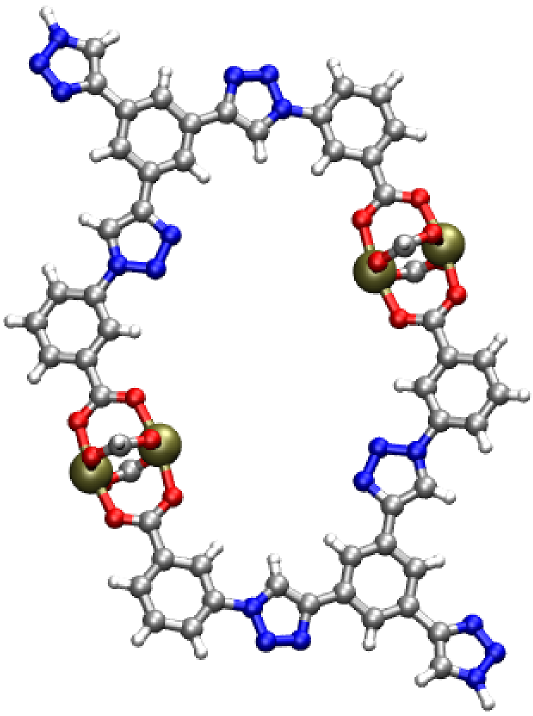

(m) Fragment 13

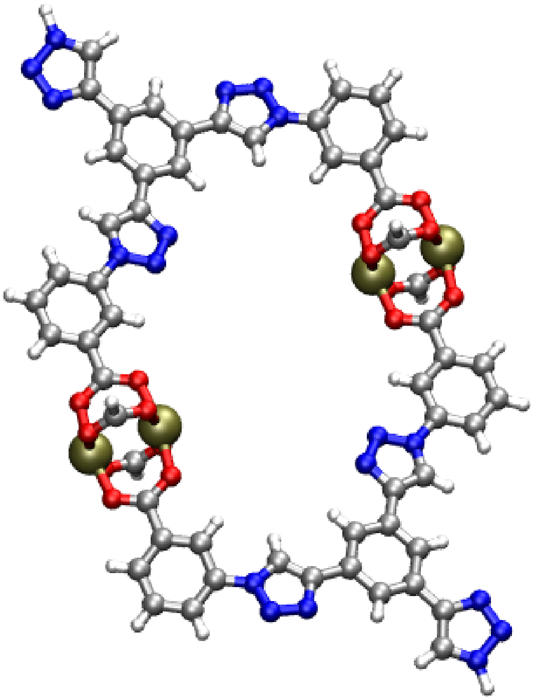

(n) Fragment 14

Table S2. The partial charges (e^-) for the chemically distinct atoms in Cu-BTTI that were used for the simulations in this work. Label of atoms correspond to Figure S2.

Atom	Label	q (e^-)	Atom	Label	q (e^-)
Cu	1	0.87626	C	39	-0.07820
Cu	2	1.20036	C	40	-0.07657
Cu	3	0.88939	C	41	-0.09656
Cu	4	1.21401	C	42	-0.22290
O	5	-0.69722	C	43	-0.52582
O	6	-0.67254	C	44	0.49787
O	7	-0.71918	C	45	-0.23221
O	8	-0.73805	C	46	0.04016
O	9	-0.70345	C	47	0.93239
O	10	-0.67199	C	48	-0.14580
O	11	-0.68040	C	49	0.04523
O	12	-0.72924	C	50	0.95111
O	13	-0.72847	C	51	-0.10670
O	14	-0.67452	C	52	-0.09220
O	15	-0.73527	H	53	0.19885
O	16	-0.72337	H	54	0.27048
C	17	-0.06237	H	55	0.09291
C	18	-0.15237	H	56	0.12790
C	19	-0.49908	H	57	0.16869
C	20	0.48514	H	58	0.20826
C	21	-0.24194	H	59	0.26538
C	22	-0.00704	H	60	0.09832
C	23	0.90111	H	61	0.14633
C	24	-0.14543	H	62	0.18324
C	25	0.02220	H	63	0.21127
C	26	0.97700	H	64	0.25086
C	27	-0.18403	H	65	0.08606
C	28	-0.03347	H	66	0.11392
C	29	-0.15213	H	67	0.18320
C	30	-0.15607	N	68	0.47164
C	31	-0.51757	N	69	-0.26426
C	32	0.44050	N	70	-0.32959
C	33	-0.17816	N	71	0.51610
C	34	-0.01321	N	72	-0.27879
C	35	0.87666	N	73	-0.31529
C	36	-0.04933	N	74	0.54142
C	37	-0.06457	N	75	-0.28168
C	38	0.90556	N	76	-0.36095

Table S3. The partial charges (e^-) for the four chemically distinct Cu^{2+} ions in Cu-BTTI as calculated using the extended charge equilibration (EQ_{eq}) method.[22] Label of atoms correspond to Figure 2.

Atom	Label	q (e^-)
Cu	1	0.90400
Cu	2	0.90500
Cu	3	0.91425
Cu	4	0.90650

Sorbate Potentials

Table S4. Parameters used to characterize the three CO_2 potentials considered in this work: TraPPE,[23] CO_2-PHAST,[24] and CO_2-PHAST*.[24] OS refers to the off-atomic sites and r corresponds to the distance from the center-of-mass (COM).

Model	Atomic Site	r (Å)	ϵ (K)	σ (Å)	q (e^-)	α° (Å^3)
TraPPE	C	0.000	27.00000	2.80000	0.70000	0.00000
	O	1.160	79.00000	3.05000	-0.35000	0.00000
CO_2-PHAST	C	0.000	8.52238	3.05549	0.77106	0.00000
	O	1.162	0.00000	0.00000	-0.38553	0.00000
	OS	1.091	76.76607	2.94473	0.00000	0.00000
CO_2-PHAST*	C	0.000	19.61757	3.30366	0.77134	1.22810
	O	1.162	0.00000	0.00000	-0.38567	0.73950
	OS	1.114	46.47457	2.99429	0.00000	0.00000

Table S5. Parameters used to characterize the four H_2 potentials considered in this work: Buch,[25] Darkrim Levesque (DL),[26] Belof Stern Space (BSS),[27] and Belof Stern Space Polar (BSSP).[27] OS refers to the off-atomic sites and r corresponds to the distance from the center-of-mass (COM).

Model	Atomic Site	r (Å)	ϵ (K)	σ (Å)	q (e^-)	α° (Å^3)
Buch	COM	0.000	34.20000	2.96000	0.00000	0.00000
DL	COM	0.000	36.70000	2.95800	-0.93600	0.00000
	H	0.370	0.00000	0.00000	0.46800	0.00000
BSS	COM	0.000	8.85160	3.22930	-0.74640	0.00000
	H	0.371	0.00000	0.00000	0.37320	0.00000
	OS	0.329	4.06590	2.34060	0.00000	0.00000
BSSP	COM	0.000	12.76532	3.15528	-0.74640	0.69380
	H	0.371	0.00000	0.00000	0.37320	0.00044
	OS	0.363	2.16726	2.37031	0.00000	0.00000

Grand Canonical Monte Carlo

Simulations of CO_2 and H_2 sorption in Cu-BTTI were performed using grand canonical Monte Carlo (GCMC)[28] on a single unit cell of the MOF. The simulations utilized the crystal structure that was reported in reference 1. This method keeps the chemical potential (μ), volume (V), and temperature (T) of a simulation box containing the MOF–sorbate system fixed while allowing other thermodynamic quantities, such as the particle number (N), to fluctuate.[28] The simulation involves randomly inserting, deleting, translating, or rotating a sorbate molecule within the simulation box with each trial move accepted or rejected based on a random number generator scaled by the energetic favorability of the move. This continues until equilibrium is reached at the desired state point. A macroscopic crystalline environment was approximated by periodic boundary conditions with a spherical cut-off corresponding to half the shortest system cell dimension length. All MOF atoms were held fixed at their crystallographic positions for the simulations.

The average particle number ($\langle N \rangle$) was calculated numerically using a statistical mechanical expression based on the grand canonical ensemble.[29,30] μ for CO_2 and H_2 was determined for a range of temperatures and pressures through the Peng-Robinson[31] and BACK[32] equations of state, respectively. For simulations using polarizable potentials,[24,27] the total potential energy (U) was calculated through the sum of the repulsion/dispersion, stationary electrostatic, and many-body polarization energies. These were calculated through the Lennard-Jones 12–6 potential,[4] Ewald summation[8,9] of the point partial charges, and a Thole-Applequist type model,[12–15] respectively. U for simulations utilizing electrostatic (nonpolarizable) potentials[23,24,26,27] contained just the first two energetic terms, while only the repulsion/dispersion energy was calculated for simulations using a single–site H_2 model.[25]

For simulations of H_2 sorption at 77 and 87 K, quantum mechanical dispersion effects were included semiclassically through Feynman–Hibbs corrections to the fourth order according to the following equation:[33]

$$U_{FH} = U + \frac{\beta \hbar^2}{24\mu_m}\left(U'' + \frac{2}{r}U'\right) + \frac{\beta^2 \hbar^4}{1152\mu_m^2}\left(\frac{15}{r^3}U' + \frac{4}{r}U''' + U''''\right) \tag{1}$$

where β is the inverse temperature, $\hbar$ is the reduced Planck's constant, μ_m is the reduced mass, and the primes indicate differentiation with respect to pair separation r.

The theoretical Q_{st} values were calculated using the following expression that is based on fluctuations in N and U:[34]

$$Q_{st} = -\frac{\langle NU \rangle - \langle N \rangle \langle U \rangle}{\langle N^2 \rangle - \langle N \rangle^2} + kT \tag{2}$$

where k is the Boltzmann constant. For all thermodynamic conditions considered in Cu-BTTI, the simulations initially consisted of 2.0×10^6 Monte Carlo steps to guarantee equilibration. The simulations continued for an additional 2.0×10^6 Monte Carlo steps to ensure reasonable emsemble averages for $\langle N \rangle$ and the Q_{st}. All simulations were performed using the Massively Parallel Monte Carlo (MPMC) code, which is currently available for download on GitHub.[35]

Simulated CO_2 Sorption Results

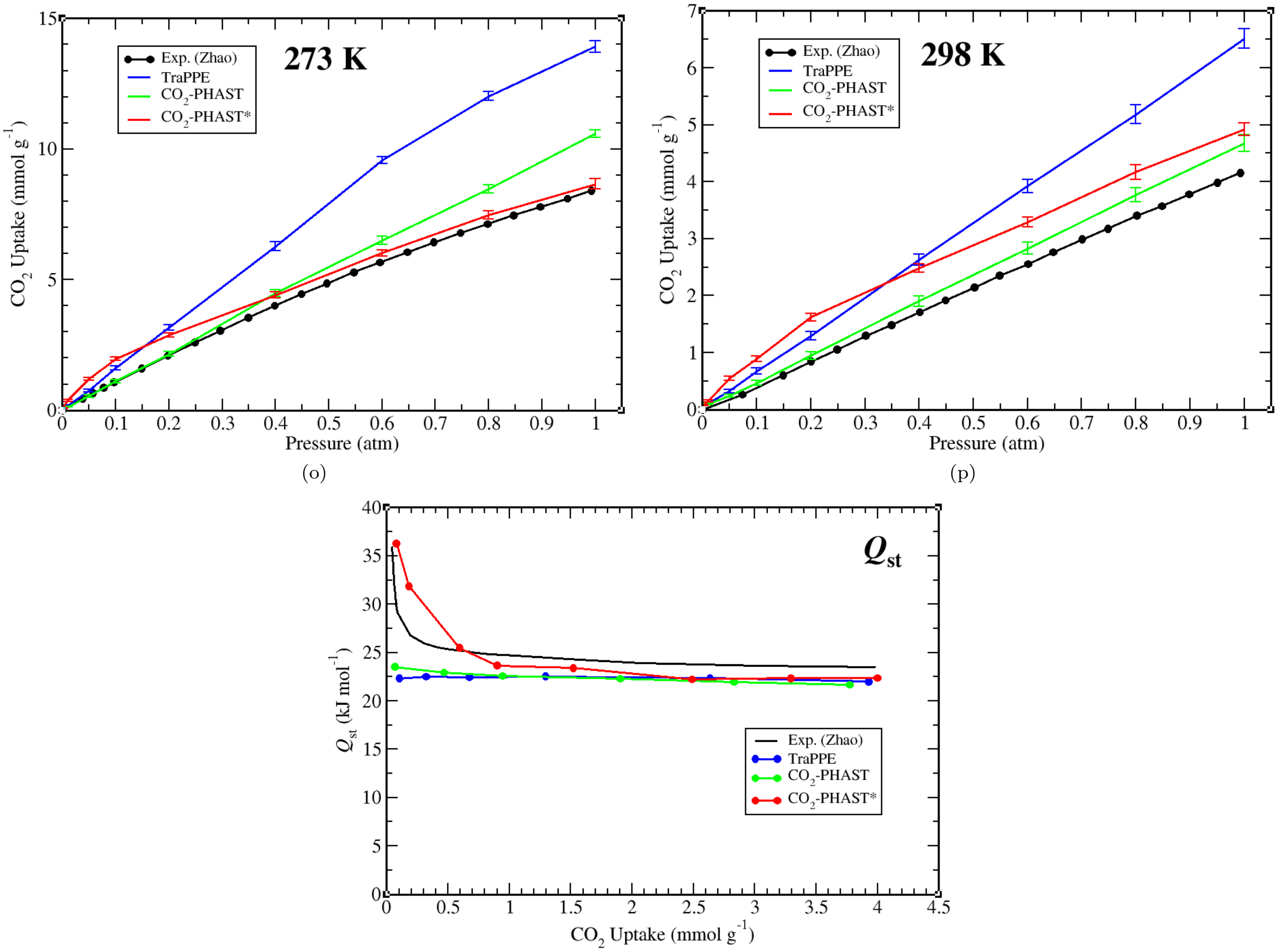

(o)

(p)

(q)

Figure S4. Low pressure absolute CO_2 sorption isotherms in Cu-BTTI at **(a)** 273 K and **(b)** 298 K, and **(c)** isosteric heat of adsorption (Q_{st}) for CO_2 as a function of loading for experiment (black) and simulations using the TraPPE (blue), CO_2-PHAST (green), and CO_2-PHAST* (red) models. The experimental data are shown from Zhao *et al.* (ref. 1).

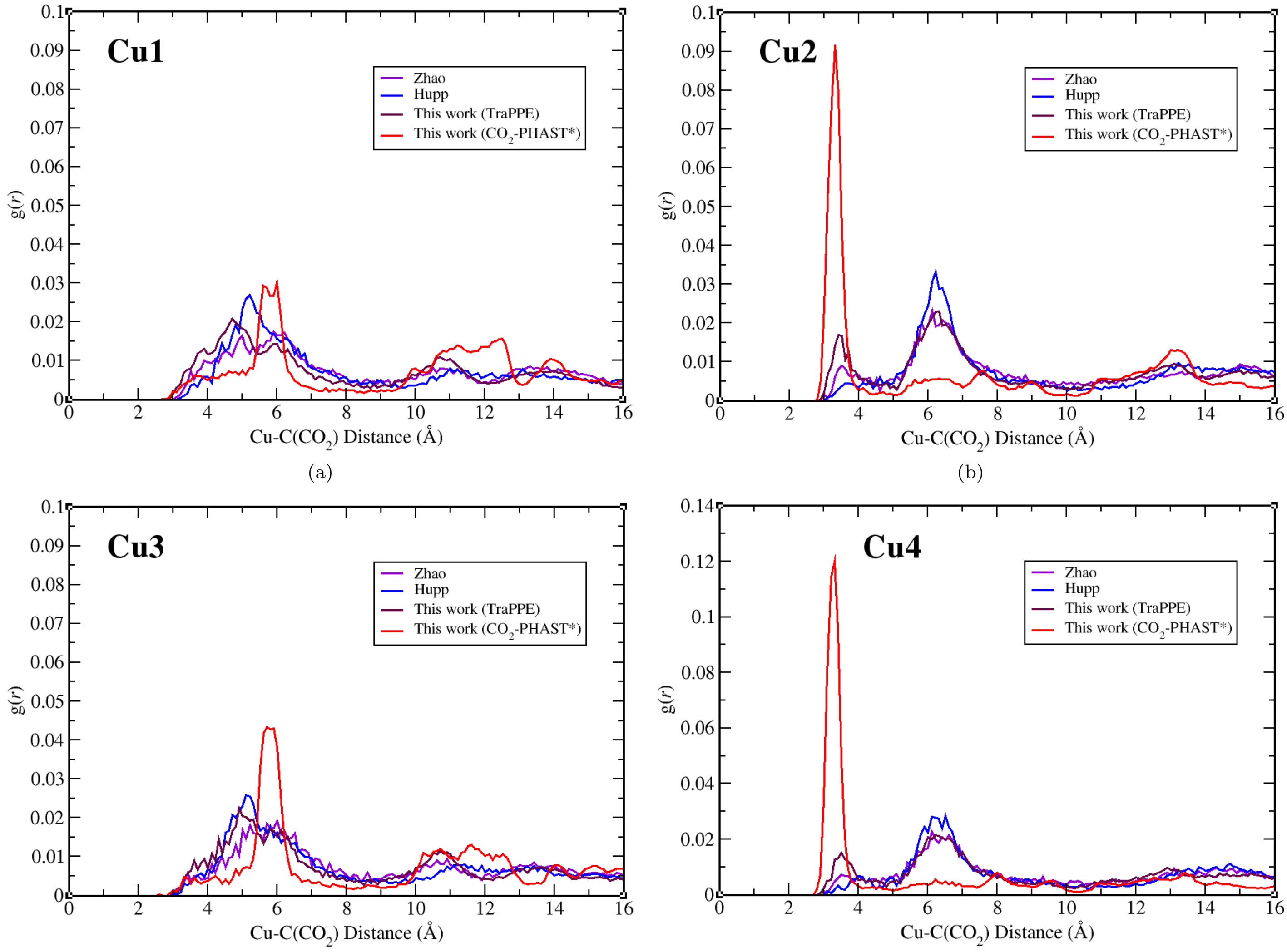

(a) (b) (c) (d)

Figure S5. Radial distribution function (g(r) of CO$_2$ carbon atoms about **(a)** the Cu1 ions (atom label 1 in Figure S2), **(b)** Cu2 ions (atom label 2 in Figure S2), **(c)** Cu3 ions (atom label 3 in Figure S2), and **(d)** Cu4 ions (atom label 4 in Figure S2) in Cu-BTTI for simulations using the TraPPE model within the potential energy function of the MOF developed by Zhao *et al.* (violet),[1] Hupp *et al.* (blue),[3] and this work (maroon) at 298 K and 0.10 atm. The results for the CO$_2$-PHAST* model at the same state point are displayed for comparison.

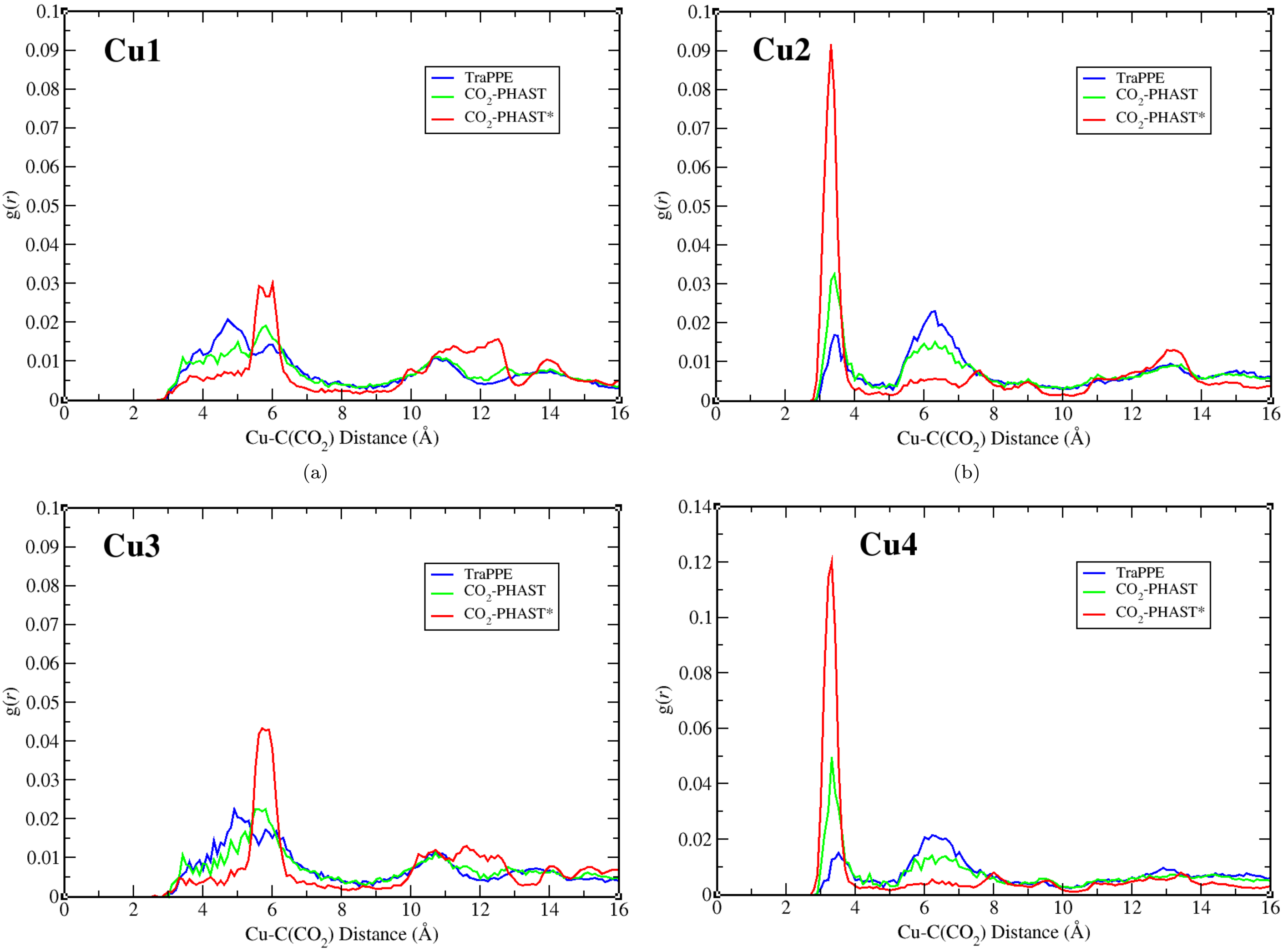

(a) (b) (c) (d)

Figure S6. Radial distribution function (g(r)) of CO_2 carbon atoms about **(a)** the Cu1 ions (atom label 1 in Figure S2), **(b)** Cu2 ions (atom label 2 in Figure S2), **(c)** Cu3 ions (atom label 3 in Figure S2), and **(d)** Cu4 ions (atom label 4 in Figure S2) in Cu-BTTI for simulations using the TraPPE (blue), CO_2-PHAST (green), and CO_2-PHAST* (red) models at 298 K and 0.10 atm.

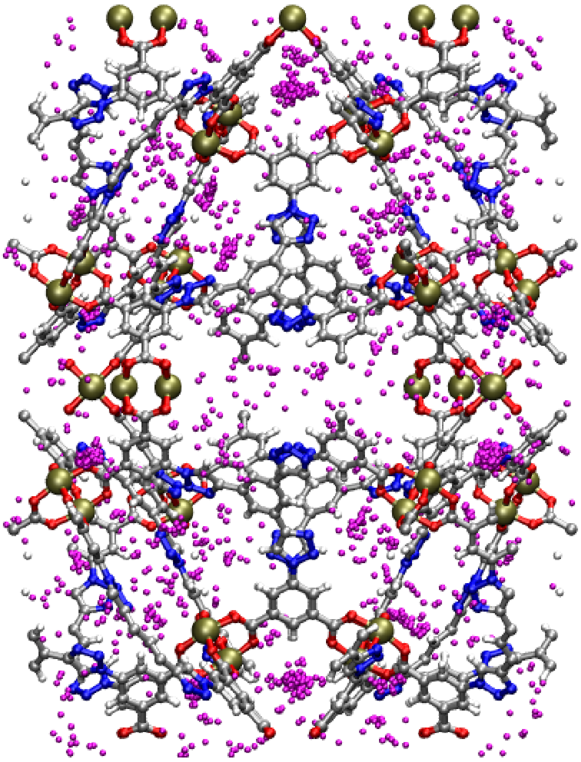

Figure S7. The a/b-axis view of the unit cell of Cu-BTTI showing CO_2 occupancy (violet) within the corners of the T–T_d cages. Atom colors: C = gray, H = white, N = red, O = red, Cu = tan.

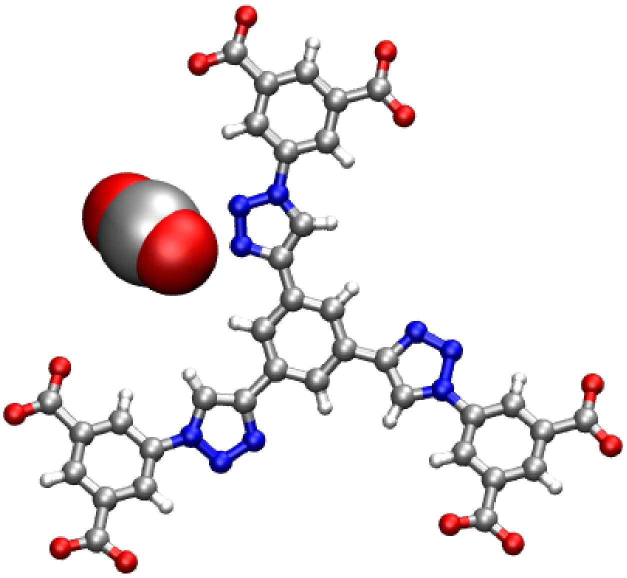

Figure S8. Molecular illustration of a CO_2 molecule sorbed onto a 1,2,3-triazole group of the BTTI linker in Cu-BTTI as determined from GCMC simulations. Atom colors: C = gray, H = white, N = red, O = red, Cu = tan.

Simulated H_2 Sorption Results

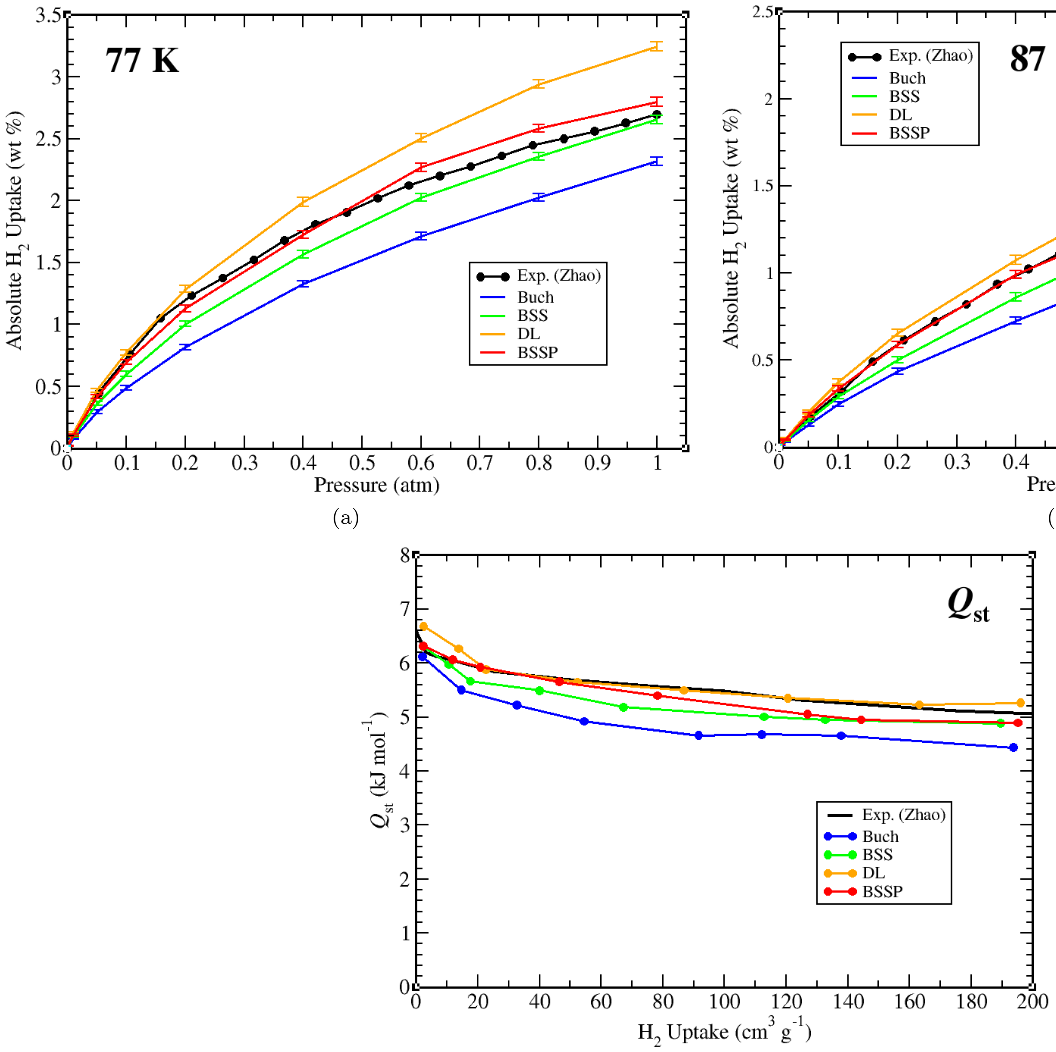

(a)

(b)

(c)

Figure S9. Low pressure absolute H_2 sorption isotherms in Cu-BTTI at **(a)** 77 K and **(b)** 87 K, and **(c)** isosteric heat of adsorption (Q_{st}) for H_2 as a function of loading for experiment (black) and simulations using the Buch (blue), BSS (green), DL (orange), and BSSP (red) models. The experimental data are shown from Zhao *et al.* (ref. 1).

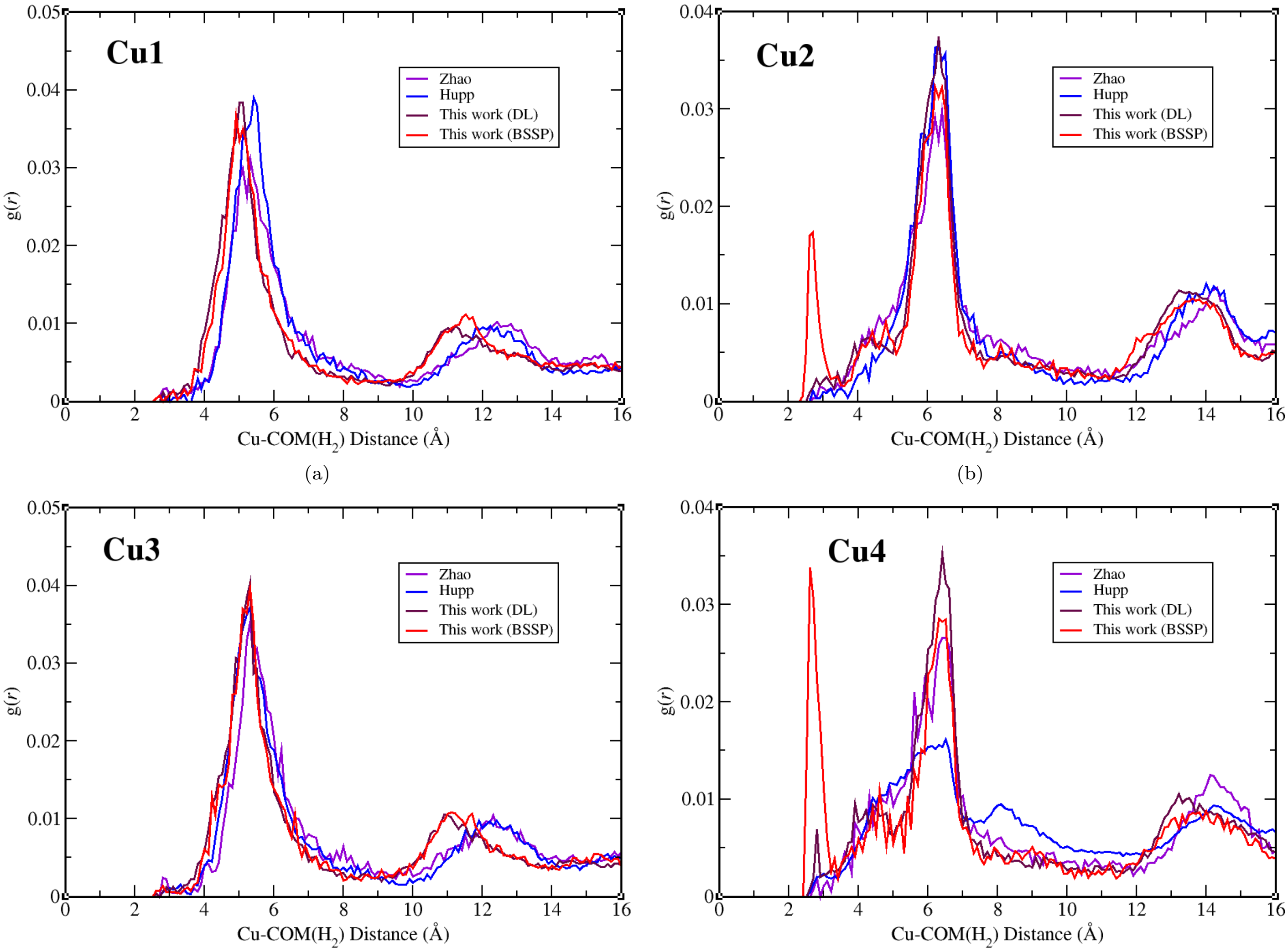

(a) (b) (c) (d)

Figure S10. Radial distribution function (g(r) of the center-of-mass (COM) of H_2 molecules about **(a)** the Cu1 ions (atom label 1 in Figure S2), **(b)** Cu2 ions (atom label 2 in Figure S2), **(c)** Cu3 ions (atom label 3 in Figure S2), and **(d)** Cu4 ions (atom label 4 in Figure S2) in Cu-BTTI for simulations using the DL model within the potential energy function of the MOF developed by Zhao *et al.* (violet),[1] Hupp *et al.* (blue),[3] and this work (maroon) at 77 K and 0.01 atm. The results for the BSSP model at the same state point are displayed for comparison.

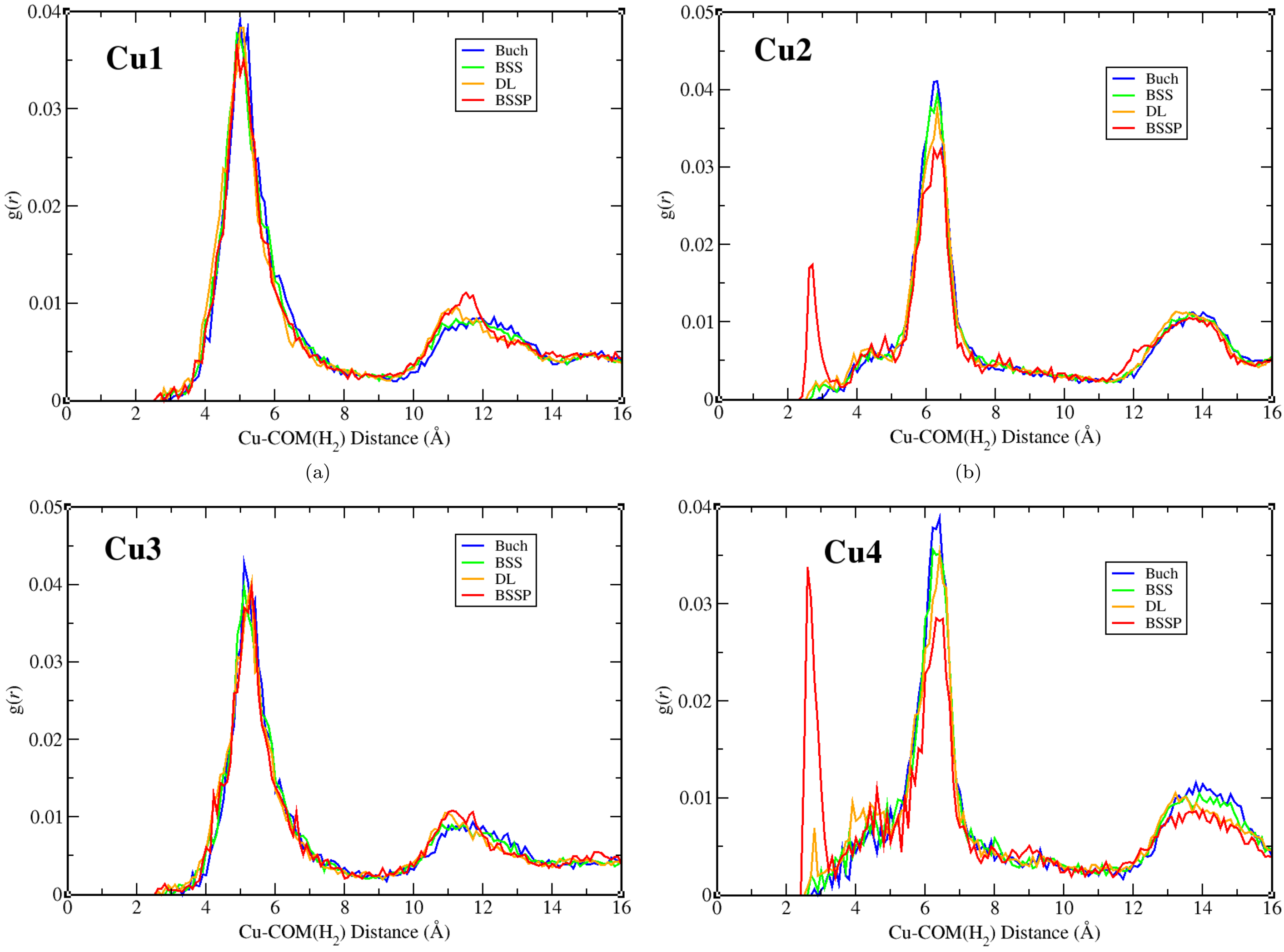

(a) (b)

(c) (d)

Figure S11. Radial distribution function (g(r)) of the center-of-mass (COM) of H_2 molecules about **(a)** the Cu1 ions (atom label 1 in Figure S2), **(b)** Cu2 ions (atom label 2 in Figure S2), **(c)** Cu3 ions (atom label 3 in Figure S2), and **(d)** Cu4 ions (atom label 4 in Figure S2) in Cu-BTTI for simulations using the Buch (blue), BSS (green), DL (orange), and BSSP (red) models at 77 K and 0.01 atm.

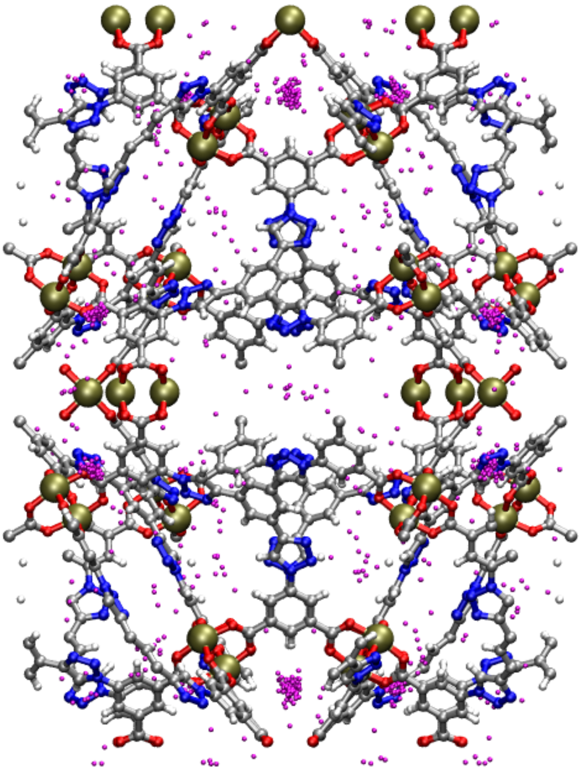

Figure S12. The a/b-axis view of the unit cell of Cu-BTTI showing H_2 occupancy (violet) within the corners of the T–T_d cages. Atom colors: C = gray, H = white, N = red, O = red, Cu = tan.

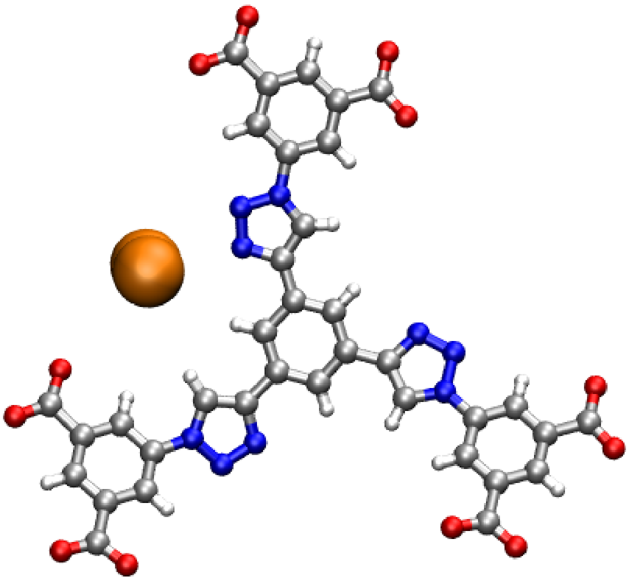

Figure S13. Molecular illustration of a H_2 molecule (orange) sorbed onto a 1,2,3-triazole group of the BTTI linker in Cu-BTTI as determined from GCMC simulations. Atom colors: C = gray, H = white, N = red, O = red, Cu = tan.

[1] X.-J. Wang, P.-Z. Li, Y. Chen, Q. Zhang, H. Zhang, X. X. Chan, R. Ganguly, Y. Li, J. Jiang and Y. Zhao, *Sci. Rep.*, 2013, **3**, 1149.
[2] Y. Yan, M. Suyetin, E. Bichoutskaia, A. J. Blake, D. R. Allan, S. A. Barnett and M. Schroder, *Chem. Sci.*, 2013, **4**, 1731–1736.
[3] C. E. Wilmer, O. K. Farha, T. Yildirim, I. Eryazici, V. Krungleviciute, A. A. Sarjeant, R. Q. Snurr and J. T. Hupp, *Energy Environ. Sci.*, 2013, **6**, 1158–1163.
[4] J. Jones, *Proc. R. Soc. A*, 1924, **106**, 463–477.
[5] W. L. Jorgensen, D. S. Maxwell and J. Tirado-Rives, *J. Am. Chem. Soc.*, 1996, **118**, 11225–11236.
[6] A. K. Rappé, C. J. Casewit, K. S. Colwell, W. A. Goddard and W. M. Skiff, *J. Am. Chem. Soc.*, 1992, **114**, 10024–10035.
[7] M. P. Allen and D. J. Tildesley, *Computer Simulation of Liquids*, Oxford University Press, Oxford, United Kingdom, 1989.
[8] P. P. Ewald, *Ann. Phys.*, 1921, **369**, 253–287.
[9] B. A. Wells and A. L. Chaffee, *J. Chem. Theory Comput.*, 2015, **11**, 3684–3695.
[10] P. T. van Duijnen and M. Swart, *J. Phys. Chem. A*, 1998, **102**, 2399–2407.
[11] K. A. Forrest, T. Pham, K. McLaughlin, J. L. Belof, A. C. Stern, M. J. Zaworotko and B. Space, *J. Phys. Chem. C*, 2012, **116**, 15538–15549.
[12] J. Applequist, J. R. Carl and K.-K. Fung, *J. Am. Chem. Soc.*, 1972, **94**, 2952–2960.
[13] B. Thole, *Chem. Phys.*, 1981, **59**, 341–350.
[14] K. A. Bode and J. Applequist, *J. Phys. Chem.*, 1996, **100**, 17820–17824.
[15] K. McLaughlin, C. R. Cioce, T. Pham, J. L. Belof and B. Space, *J. Chem. Phys.*, 2013, **139**, 184112.
[16] M. Valiev, E. Bylaska, N. Govind, K. Kowalski, T. Straatsma, H. V. Dam, D. Wang, J. Nieplocha, E. Apra, T. Windus and W. de Jong, *Comput. Phys. Commun.*, 2010, **181**, 1477–1489.
[17] W. D. Cornell, P. Cieplak, C. I. Bayly, I. R. Gould, K. M. Merz, D. M. Ferguson, D. C. Spellmeyer, T. Fox, J. W. Caldwell and P. A. Kollman, *J. Am. Chem. Soc.*, 1995, **117**, 5179–5197.
[18] W. J. Stevens, H. Basch and M. Krauss, *J. Chem. Phys.*, 1984, **81**, 6026–6033.
[19] P. J. Hay and W. R. Wadt, *J. Chem. Phys.*, 1985, **82**, 270–283.
[20] L. A. LaJohn, P. A. Christiansen, R. B. Ross, T. Atashroo and W. C. Ermler, *J. Chem. Phys.*, 1987, **87**, 2812–2824.
[21] C. M. Breneman and K. B. Wiberg, *J. Comput. Chem.*, 1990, **11**, 361–373.
[22] C. E. Wilmer, K. C. Kim and R. Q. Snurr, *J. Phys. Chem. Lett.*, 2012, **3**, 2506–2511.
[23] J. J. Potoff and J. I. Siepmann, *AIChE J.*, 2001, **47**, 1676–1682.
[24] A. L. Mullen, T. Pham, K. A. Forrest, C. R. Cioce, K. McLaughlin and B. Space, *J. Chem. Theory Comput.*, 2013, **9**, 5421–5429.
[25] V. Buch, *J. Chem. Phys.*, 1994, **100**, 7610–7629.
[26] F. Darkrim and D. Levesque, *J. Chem. Phys.*, 1998, **109**, 4981–4984.
[27] J. L. Belof, A. C. Stern and B. Space, *J. Chem. Theory Comput.*, 2008, **4**, 1332–1337.
[28] N. Metropolis, A. W. Rosenbluth, M. N. Rosenbluth, A. H. Teller and E. Teller, *J. Chem. Phys.*, 1953, **21**, 1087–1092.
[29] D. Frenkel and B. Smit, *Understanding Molecular Simulation: From Algorithms to Applications*, Academic Press, New York, 2002.
[30] D. A. McQuarrie, *Statistical Mechanics*, University Science Books, Sausalito, CA, 2000.
[31] D.-Y. Peng and D. B. Robinson, *Ind. Eng. Chem. Fundam.*, 1976, **15**, 59–64.
[32] T. Boublík, *Fluid Phase Equilib.*, 2005, **240**, 96–100.
[33] R. P. Feynman and A. R. Hibbs, *Quantum Mechanics and Path Integrals*, McGraw-Hill, New York, 1965.
[34] D. Nicholson and N. G. Parsonage, *Computer Simulation and the Statistical Mechanics of Adsorption*, Academic Press, London, 1982.
[35] J. L. Belof and B. Space, *Massively Parallel Monte Carlo (MPMC)*, Available on GitHub, 2012, `https://github.com/mpmccode/mpmc`.